AD-A105 603 FOREIGN TECHNOLOGY DIV WRIGHT-PATTERSON AFB OH F/G 20/4
ACTA MECHANICA SINICA (SELECTED ARTICLES).(U)
SEP 81 H YU, Z LI, B SUN
UNCLASSIFIED FTD-ID(RS)T-0576-81 NL

1 OF 1
AD
A105603

END
DATE
FILMED
11 81
DTIC

FTD-ID(RS)T-0576-81

(2)

AD A105603

FOREIGN TECHNOLOGY DIVISION

AIR FORCE SYSTEMS COMMAND

ACTA MECHANICA SINICA

(Selected Articles)

FOREIGN TECHNOLOGY DIVISION

Approved for public release;
distribution unlimited.

81 10 7 19

FTD-ID(RS)T-0576-81

EDITED TRANSLATION

(12) 33

(14) FTD-ID(RS)T-0576-81 (11) 8 Sep[redacted]81

MICROFICHE NR: **FTD-81-C-000816**

(6) ACTA MECHANICA SINICA (Selected Articles),

English pages: 28 (21) Edited trans. of

Source: Acta Mechanica Sinica[redacted]
pp. 68-76[redacted]

Country of origin: (China) n1 p68-76 90-95 1981.

Translated by: SCITRAN
F33657-78-D-0619

Requester: FTD/TQTA

Approved for public release; distribution unlimited.

(10) ... Yu
... Zhi
Bing-hua Sun

Accession For	
NTIS GRA&I	X
DTIC TAB	☐
Unannounced	☐
Justification	
By	
Distribution/	
Availability Codes	
Dist	Avail and/or Special
A	

THIS TRANSLATION IS A RENDITION OF THE ORIGINAL FOREIGN TEXT WITHOUT ANY ANALYTICAL OR EDITORIAL COMMENT. STATEMENTS OR THEORIES ADVOCATED OR IMPLIED ARE THOSE OF THE SOURCE AND DO NOT NECESSARILY REFLECT THE POSITION OR OPINION OF THE FOREIGN TECHNOLOGY DIVISION.	PREPARED BY: TRANSLATION DIVISION FOREIGN TECHNOLOGY DIVISION WP-AFB, OHIO.

141600

TABLE OF CONTENTS

HEAT TRANSFER STUDIES IN THE REGION OF SHOCK AND TURBULENT BOUNDARY LAYER INTERACTION INDUCED BY A CYLINDRICAL PROTUBERANCE*

Yu Hong-ru, Li Zhong-fa
(Institute of Mechanics Academia Sinica)

SUMMARY

This article describes the results of experiments on the rates of heat exchange in areas of interference associated with concave cylindrical objects. In these experiments, it has appeared that the maximum rates of heat transfer on the center line of the upper flow do not occur at the foot of the cylindrical object itself but rather, at a place about 0.1 to 0.15 times the length of the diameter of the cylinder from the base of the cylinder. In the case of a vertical cylinder, when M = 9, the largest rates of heat flow are 46 times the corresponding values for the same area when a flat plate is used instead of the cylinder. Moreover, when M = 6.6, these values are 31 times the corresponding values.

The cylinder inclination has a very large influence on the interference areas produced and on the maximum rates of heat transfer. This becomes most obvious when the Mach numbers involved are high. When one is dealing with a backward sweep of 30°, the maximum rate of heat transfer is 1/6. A forward sweep causes an increase in both the area of interference and the maximum rate of heat transfer.

1. FOREWORD

The surfaces of high speed craft and aircraft cannot avoid the necessity for the installation of various types of measuring devices, antennas and other such similar protuberances as tail fins. The

*This article was received on January 14, 1980.

blunt forward edges of these protuberances produce interference between the surface boundary layers of the aircraft or spacecraft involved and the bow-shaped detached shock waves. The occurrence of flow separation and reattachment causes a great increase in the heating rate in the neighboring areas as compared with a situation in which there is no protuberance and this is particularly true when the Mach numbers involved are high. Due to the complexity of this type of three-dimensional shock wave-boundary layer interference flow field, it is first necessary to make experimental observations and measurements in order to make clear the principles which govern these interference flow fields and their new phenomena. This sort of initial work makes it easier to construct appropriate flow models.

Concerning the typical sorts of cylindrical protuberences, this matter has drawn the attention of quite a few researchers. However, most of them have concentrated on the clear representation of the surface flow spectra caused by turbulence as well as on the area influenced by this turbulence [1-5]. Turbulence flow interference heat transfer experiments have been limited to the supersonic realm [6]. The Mach number of the gas flow involved has a very important influence on the interference area heat transfer. High Mach number three-dimensional shock wave turbulence flow boundary layer interference heat transfer experiments are very important.

The area of the most severe increase in heat is located in the base of the cylinder. The heat flow distribution at this point changes dramatically. If one does not carefully position the point at which measurements are taken, it is difficult to measure accurately the peak values and the positions of these values. This article puts its main emphasis on the research into the heat transfer distribution characteristics of this area of severe increases in heat.

In the winter of 1977, when we were running experiments at Mach number M = 9 conditions, we made complete measurements of the heat flow rates on the surfaces around cylindrical protuberences. We found that the maximum surface heat flow rates on the center line of the upper flow of the cylinders considered were located at a point approximately 1/10 the diameter of the cylinder from the surface of the cylinder. The maximum values which were measured were far higher than the numerical values which were obtained by calculations based on empirical formulae [7,8] currently in use in China and overseas. Due to the fact that, at that time, we were using plug type sensors, these sensors suffered from the limitations of their dimensions (diameter 5.5mm); moreover, the placement of these sensors was relatively sparse. These experiments made use of changes in the diameter of the cylinders involved and results were only obtained after non-dimensional processing with the diameter of the cylinder involved as the basis. In order to verify the accuracy of this set of principles for describing the heat transfer parameter distributions involved as well as the accuracy of the data offered, a new series of tests was run in 1978 after the test production of a new sensor (width 0.5mm, sensor interval 2mm). Due to the relative density of the distributed sensor points, the maximum values which were measured for the surface heat flow rates were approximately 20% higher than those measured during the previous tests. The maximum surface heat flow rates, compared to those measured when there was no concave protuburence present and measured for the same positions with a flat plate installed, were 46 times higher. In order to observe the influence of the gas flow Mach number, in 1979, another set of supplementary experiments were carried out with M = 6.6. This article gives an overall description of the results of these experiments with special emphasis on the various types of phenomena which appeared in these experiments.

2. A DESCRIPTION OF THE EXPERIMENTS

Experimental equipment. These experiments were carried out in the JF8 shock wave wind tunnel. The test section was 6.5m long, and the test length was 13.3m. The internal diameter in both cases was 150mm. The semi-angle for the cone-shaped jet tube was $7\frac{1}{8}°$. The jet tube exhaust diameter and the diameter of the experimental section were the same, 1.2m.

The experimental gases were air and use was made of two types of operational conditions. The first of these was a reverse jet model of operation. The total pressure in the storage chamber was 420 bars. The total temperature was 950°K, and the Mach number of the gas flow in the experiments was 9. The Reynolds number was 4.5×10^7 per meter. The other operation made was the straight through mode. In this mode, the storage chamber total pressure was 45 bars. The total temperture was 680°K. The Mach number of the gas flow in the experiment was 6.6 and the Reynolds number was 1.8×10^7 per meter. The duration of the experiments was always 4 milliseconds. According to theoretical predictions, at the place where the protuburence was installed, the boundary layer of the flat plate would respectively have thicknesses of 5.3 and 4.4mm.

Measurement systems. The rates of surface heat flow for the flat plate were measured by the use of platinum plated electrical resistance temperature devices. The measurement signal passed through the thermoelectric simulation net and was changed into a signal which was in direct proportion to the heat flow. After this was done [9], it was recorded by means of oscilloscope photography. The data was displayed in comparison form. This was done in order to get rid of the error introduced by the measurement system itself. That is to say, before the protuburence was installed, experiments were conducted to measure the flat plate surface heat flow rate for the location in question. After this was done, a comparison was carried out with the surface heat flow rates measured after the protuburence was installed and the value of the ratio of these

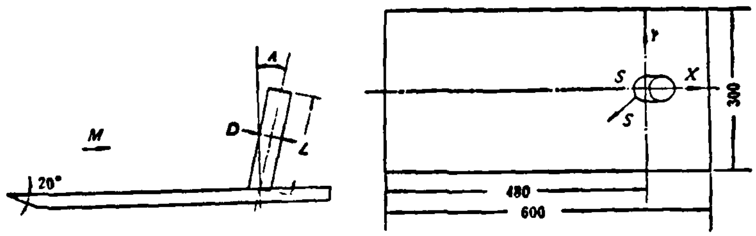

Figure 1. Model flat plate dimensions and symbols.

two values was solved for.

Models. When one compares convex protuburences and aircraft or spacecraft, the dimensions of the former are much smaller. If one makes use of a scale for geometric reduction, the dimensions of a convex protuburence on a model would be too small. This makes experimental observations as well as the placement of sensors difficult to carry out. In response to these problems, we took a flat plate on the surface of the spacecraft or aircraft involved and in the vicinity of the convex protuburence involved and used this to simulate the protuburence on the model. The Mach number was also simulated with the Mach number for the local area of the craft model in which the protuburence was supposed to appear. In this way, the dimensions of the convex protuburence on the flat plate of the model could be much larger. The external dimensions of the flat plate simulation used in these experiments as well as various types of symbols are presented in detail in Figure 1. The flat plate was installed with an agle of attack of zero, and in its leading edge for 20mm a 2x2mm horizontal convex trench was opened. This was to facilitate the turning of boundary layers.

Concerning the oil flow visualization technique, the process of starting up a shock wave wind tunnel is fast. As far as the

reverse jet operational configuration used in these experiments goes, the duration of the experiments was immediately stopped by the sparseness of the reflected jet in the test section. Because of this, the process of stopping is also very fast. Basically, surface oil flow flow spectra are formed by the effects of gas flow during the duration of the experiments. Although the duration of the experiments was very short, the oil flow flow spectrum for the inside of the area close to the cylinder on which surface there are exerted large shear forces stands out very clearly. The paint type material used in the oil flow technique is diffusion pump oil with a blackening powder added. Before the experiments, the paint type material was spread evenly on the surface of the flat plate. After the experiments, the flow spectrum remained. Under conditions in which $M = 4$, the standard oil flow flow spectrum is as shown in photograph 1 (for the photographs in this article see Plate I).

3. RESULTS OF EXPERIMENTATION AND DISCUSSION

1. The principles governing the distribution of heat transfer parameters in long vertical cylinders. On the basis of research done on the oil flow flow spectra of surfaces [3] as well as on the results of observations made in these experiments, it is possible to obtain the interference effects which cylindrical protuburences have with flat plate surfaces. When the length to diameter ratio is $L/D \geqslant 5$, it is possible to consider the cylinder as unlimited in length. Concerning the long cylinders presented in this article, their length to diameter ratios were all equal to or larger than 5.

On the center line of flow over protuburences, there are two types of Mach number ($M = 6.6$ and 9) vertical cylindrical heat transfer parameter distribution curves which are shown in Figure 2. (h_0 is the flat plate heat transfer coefficient at measurement points where there are no protuburences). The basic characteristics

of these distribution curves are as follows. Beginning from the vicinity of the place at which interference starts, the heat transfer parameters gradually increase. After maintaining a steady plateau, these values drop. After this, from their lowest point, there is a sudden rise to their peak values. After passing these peak value points, the values then go back to a monotonously steady decline. In order to take the surface sections of the neighboring columns and represent their curves more clearly, one can use logarithmic coordinates, and the area close to the columns in question are expanded as shown in Figure 3. From this figure, it can be seen that the location of the peak values is at a place from 0.1 to $0.15D$ from the surface of the column involved.

The form of the heat transfer coefficient curves discussed above can go together with the interference flow field structures which can be deduced on the basis of surface oil flow flow spectra (Plate 1) and Schlieren photography (photograph 2(a)) in order to add to an overall explanation. There is a group of compression waves in existence at the place where the oblique shock waves caused by the interference of protuburences and the boundary layers of the flat plate involved. The curves defined by the coefficients of heat transfer begin their gradual rise at this point. Later, these curves come under the influence of the oblique shock waves involved and, because of this, they maintain a long level configuration in this later section. Even later on, they become subject to the influence of vortices at the base of the protuburences involved. Close by the upper reaches of these vortices, there is the transition area in the direction of flow speed change. The flow speeds are very low and, because of this, a trough section of the curves appears. Close by the base section of the protuburences involved and under the influence of the vortices we have mentioned, the coefficients of heat transfer rise very fast. Due to the fact that the base section of the protuburences involved are sharp right angle turns, these vortices are not able to directly exert their influence on the base section of the protuburences. Because of this,

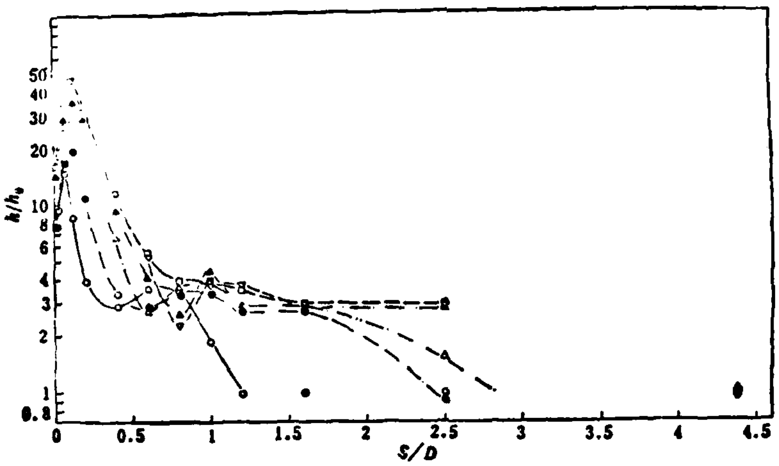

M = 9, Re = 4.5×10⁷/ meters

2

○ 代表 L/D = 0.25; △ 代表 L/D = 1.0; □ 代表 L/D = 3.0;
● 代表 L/D = 0.50; ▲ 代表 L/D = 2.0; ▽ 代表 L/D = 5.0.

Figure 2. Heat transfer coefficient distribution on the center line of the upper reaches of vertical column flow.

key: 2-- for

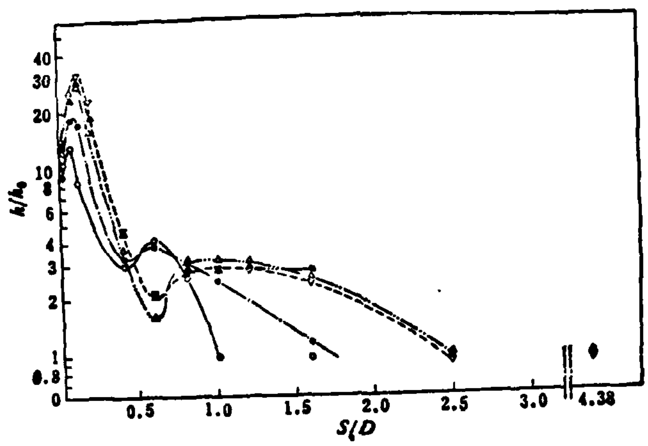

M = 6.6, Re = 1.8×10⁷/meters

Figure 2 (continued)

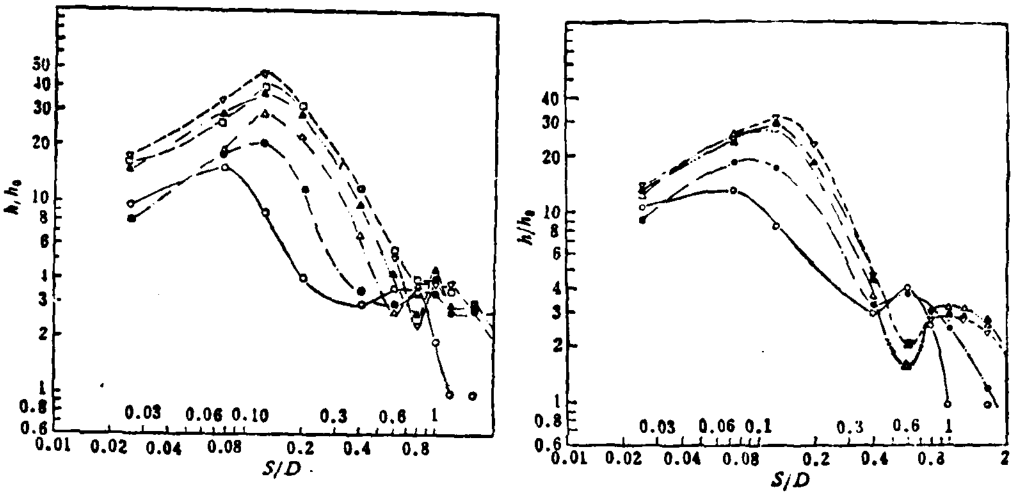

M = 9, Re = 4.5×10⁷/ meters   M = 6.6, Re = 1.8×10⁷/ meters

Figure 3. Distribution of heat transfer coefficients in the area near the columns involved on the center line of the upper reaches of round vertical columns.

the peak values are located at a fixed distance from the base section of them.

From the surface oil flow flow spectra (plate 1), it is possible to observe the dimensions of the vortices on the surface of flat plates involved. From the Schlieren photography (Photograph 2a), it is possible to make out the thickness of the vortices involved in a vertical direction. The black belt on the upper boundary is a shear layer. This vortex is influenced by high pressure coming from three different directions, and this condition is produced by the downwash flow which adheres closely to the surface of the columns involved. There is a strong relationship between the strength of the vortices concerned and the Mach number of the gas flow. The higher the Mach numbers involved are for the gas flows concerned, the higher is the strength of the vortices and, because of this, the higher are the peak values for the heat transfer coefficients.

If one makes a comparison with two-dimensional forward stepped heat transfer coefficient distribution curves [10], one will find similar configurations. However, the range of disturbance is much

smaller than that of the two-dimensional stepped case and, because of this, the values for the peak heat transfer coefficients are much higher.

Lateral heat transfer coefficient distribution curves for vertical columns are shown in Figure 4. They are the same as those for the upper center lines and the peak value points are also located a certain fixed distance from the surface of the columns involved. This distance is greater than the distance from the upper center line. However, the gradient in the vicinity of the peak values is smooth and gentle. The peak values, in this case, are clearly lower than the peak values for the center line of the upper parts. In fact, they are almost only 1/3 of the latter.

The horizontal distribution curves for the lower center of a column at a distance one radius of the column from it are shown in Figure 5. At the intersection points on the center line, the coefficients of heat transfer for long columns and the coefficients of heat transfer for non-columner flat plates are quite close to each other. The coefficients of heat transfer toward the outside decrease and, at the location 0.2D from the center line, they fall to approximately half of the flat plate values. Starting from this value, they begin to slowly heat up to their peak values. After passing their peak values, they very slowly drop down again. These peak values only have about 1/7 of the peak values on the center line of the upper parts of the flow; however, they are still several times the values which one gets for a flat plate. Because of changes of this sort are very slow, the width of the band of heat increase and the total amount of temperature increase are still not low.

2. <u>An empirical formula for the maximum heat transfer coefficient value for long vertical columns</u>. The maximum heat transfer coefficients for the flat plate interference area appear on the

center line of the upper flow. Cline [7]. on the basis of experimental data, ($2.4 \leqslant M \leqslant 4.44$), and the following empirical formula is obtained

$$h_{max}/h_0 = 22M\ Re^{1/5} \tag{1}$$

In this equation, the magnitude of the calculated Reynolds number is the immersed length of the flat plate. If one makes a comparison of values for the heat transfer coefficients at their highest values calculated according to the formula presented above in these experiments, as far as $M = 9$ is concerned, the value is 15.7. For $M = 6.6$, it is 13.3. The deviations of 46 and 31 from the measured values is quite considerable. And the deviation between the compared values are not the same either. It appears that this formula is not suitable for high Mach numbers.

Truitt [8] takes the center line flow and considers it a two-dimensional flow, so that he derives the relationship presented below,

$$h_{max}/h_0 = (1 + K_2 M)^{9/5}/Re^{1/5} \tag{2}$$

On the basis of experimental data, we get a precise determination of $K_2 = 25$. A comparison of the curves involved is shown in Figure 6. In the same figure, one also sees the 4B-128 data from reference [7]. It can be seen from this figure that the Burbank [6] data and other data of a similar sort are wrong on the low side. There are two reasons for this. One is the scarcity of measurement points (round columns with D = 2.8" and an interval between sensors of 1"). This scarcity makes it impossible for accurate measurements to be made of the actual peak values. The second reason is that because we used a tin stainless steel shell to measure heat flow, it was not possible to correct for the relatively large errors introduced because of lateral heat diffusion. On the basis of the analysis of George [11], the error which is caused by laterally induced heat flow when one uses thin shells for measurement purposes is

$$\frac{\text{rate of laterally induced heat flow}}{\text{rate of surface heat flow}} \simeq \alpha t \frac{\nabla^2 \dot{Q}}{\dot{Q}} \qquad (3)$$

In this equation, α is the coefficient of thermal conductivity. t is the measurement time. $\dot{Q}$ is the rate of heat flow on the surface. On the basis of the heat transfer coefficient distribution curves obtained in these experiments, the place at which one gets the estimated peak value for heat flow, that is, $\nabla^2\dot{Q}/\dot{Q}$ is on the order of 10 and the value for stainless steel of α = 0.05 cm^2/sec. The laterally induced heat flow error which comes from the use of thin shells is capable of reaching a value several times the result. Due to the fact that the place at which the peak value occurs, that is $\nabla^2\dot{Q}/\dot{Q}$, is a function of the Mach number of the gas flow involved, when this number is reduced, the peak values quickly drop. Because of this, when the Mach numbers involved are low, the laterally induced heat flow error is small. In Figure 6, the error revealed in a comparison between M = 2.4 and 2.65 type numerical data and data obtained when M = 3.51 and 4.44 was small; this phenomenon is probably related concerning cases in which one uses thin film electrical resistance temperature measuring devices to measure heat flows, due to the fact that the low value ($\alpha \sim 0.008$ cm^2/sec) is extremely low, the reaction is fast, and the measurement interval is pushed forward in time. Even if one takes his measurements at the place at which the heat transfer distribution is extremely pointed, the error from lateral heat conduction will still be very low.

3. <u>The influence of the height of the cylinder</u>. From Figure 3, it can be seen that, whether M = 9 or M = 6.6, when the height-to-radius ratio is $L/D \geqslant 1$, the configurations of heat transfer coefficient curves on the center line of the upper reaches of flow for different height-to-radius ratios are similar, and the curves conform closely to one another. When $L/D < 1$, despite the fact that the configurations of the curves are similar, the horizontal

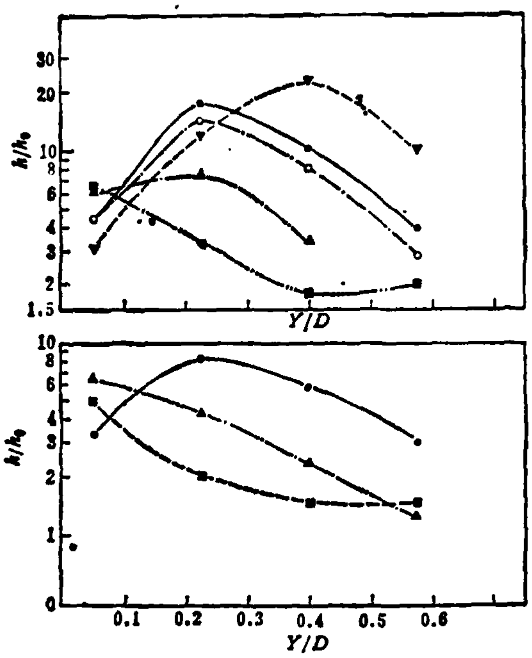

1 上图 $M=9$, $Re=4.5\times10^7$/米 2 3 下图 $M=6.6$, $Re=1.8\times10^7$/米 4

5 ● 代表垂直长柱; 6 ▲ 代表后掠 15° 长柱; 7 ■ 代表后掠 30° 长柱;

8 ▼ 代表前倾 15° 长柱 9 ○ 代表 $L/D=1$ 垂直柱

Figure 4. Lateral heat transfer coefficient distributions for long colums (X/D=0 cross section)

Key: 1--top graph; 2--meter; 3--bottom graph; 4--meter; 5--represents long vertical columns; 6--represents long cylinder swept back by 15°; 7--represents long cylinder swept back by 30°; 8--represents long cylinder swept forward by 15°; 9--represents vertical columns for L/D=1

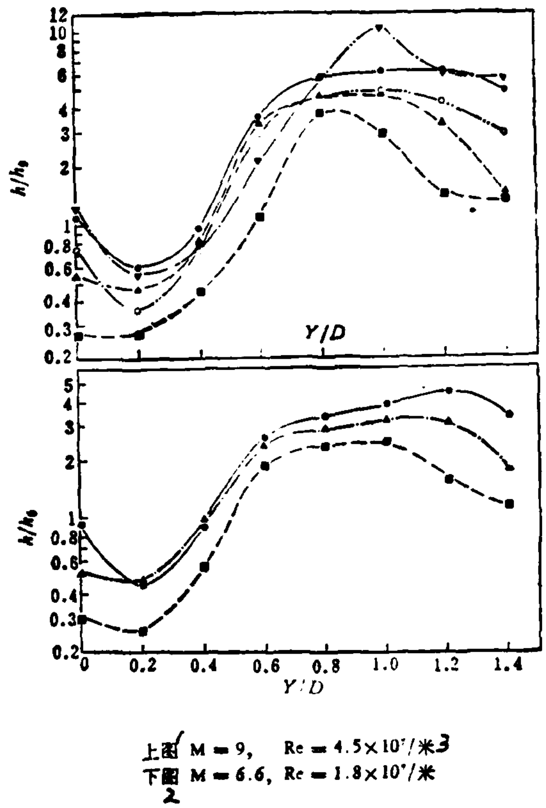

Figure 5. Heat transfer coefficient distributions for the rear sections of long cylinders (L/D=1 cross section)

Key: 1--top graph; 2--bottom graph; 3--meter

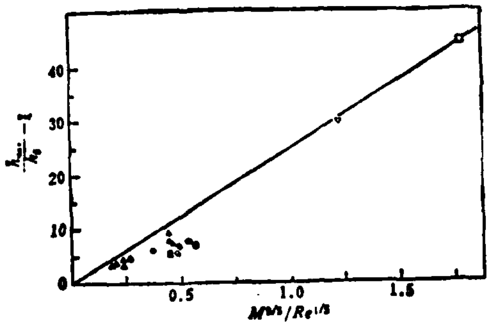

— $\frac{h_{max}}{h_0} - 1 = 25\,\frac{M^{9/5}}{Re^{1/5}}$

○ M = 4.44, ○ M = 3.51, ▲ M = 2.65 } 文献[6]
▲ M = 2.4 文献[7]
□ M = 9 本文
▽ M = 6.6 本文

Figure 6. The relationship between the conditions of the incoming flow and the maximum heat transfer coefficients for long cylinders.
1--references; 2--case

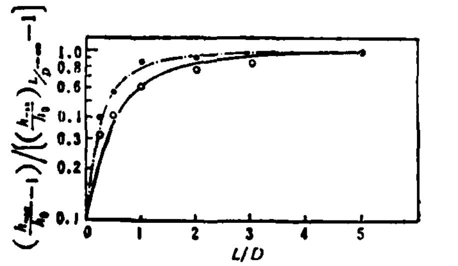

$\frac{h_{max}}{h_0} - 1 = \left[\left(\frac{h_{max}}{h_0}\right)_{L/D\to\infty} - 1\right]\left[1 - e^{-K_1\frac{L}{D}}\right]$

○ M = 9 $K_1 = 1$
● M = 6.6 $K_1 = 1.6$

Figure 7. The influence of height-to-radius ratio on the maximum heat transfer coefficients for the center line of the upper parts of the flow.

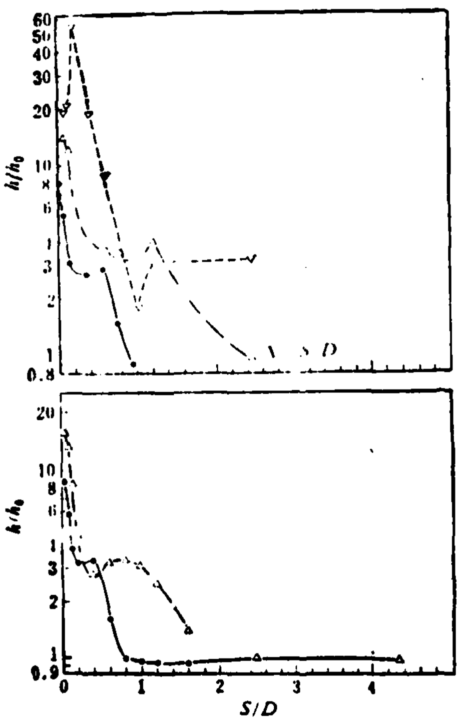

Figure 8. Heat transfer coefficient distribution for the center lines of the upper parts of flow in the case of long columns with forward oblique angles and sweepback angles.

上图 M = 9, Re = 4.5×10⁷/米
下图 M = 6.6, Re = 1.8×10⁷/米
● 后掠 30°; ▲ 后掠 15°; ▼ 前倾 15°.

1--top graph; 2--meter; 3--bottom graph; 4--sweepback angle; 5--forward oblique

dimensions have been foreshortened, and there is an obvious drop which also occurs in the peak values for the heat transfer coefficients.

As was said above, the heat transfer coefficients for the flat surfaces adjacent to protuburences are strongly dependent on the dimensions and strengths of the vortices involved. When the height of a column is smaller than its radius, the Y-point is not far from the apex. The high pressures in the vicinity of the Y-point leaks off the apical point early and this causes a reduction in both the dimensions and the strength of the vortices involved. Because of this, the differences between the heat transfer curves for the various height cases are not great.

The curves which are defined by the influence of the height-to-radius ratio of cylinders on the maximum heat transfer coefficients on the center line of the upper parts of the flow are drawn out in Figure 7. The influence of height-to-radius ratios indicate weakening and attenuation and inductions can be made of the type of empirical formula presented below, that is,

$$\frac{h_{max}}{h_0} - 1 = \left[\left(\frac{h_{max}}{h_0}\right)_{\frac{L}{D}\to\infty} - 1\right]\left[1 - e^{-K_1 \frac{L}{D}}\right] \qquad (4)$$

There is a relationship between K_1 and the Mach number of the gas flow involved. In these expeirments, when $M = 9$, $K_1 = 1.0$, and when $M = 6.6$ then $K_1 = 1.6$.

4. <u>The influence of the angle of inclination in cylinders</u>. The influence of sweepback angle and forward sweep angles have on the curves defined by the heat transfer coefficient distribution along the center lines of the upper parts of flow are very large (Figure 8). First of all, a sweepback angle changes the configuration of these distribution curves. Even if the sweepback angle

is 15°, the distribution curves involved will already show a change from the base section outward in the form of a monotonous decline; however, there will still be a trough. When the angle of sweepback involved is 30°, the trough will also disappear. After this, angles of sweepback cause the areas influenced by interference to be greatly reduced in size. The most important thing is that the heat transfer coefficients are greatly reduced.

A sweepback angle configuration is an effective measure to use in order to improve the interference heating environment. It is at its most effective when Mach numbers are high. The use of configurations swept forward was found to be without any use at all as far as improving the heating environment on flat plate surfaces goes. Due to the strengthening of the high pressure downwash, there is not only a rise in the peak values of heat transfer coefficients, but also an expansion in the range of interference.

The influence which a sweepback angle configuration has on the heating environment of flat plate surfaces can explain the wave graphs which appear in the Schlieren photographs concerned, plates 2a, b and c. If one is considering the case of vertical columns, the bow-shaped shock waves above Y-points are parallel to the surface of the cylinders, and the gas flow behing these waves are perpendicular to the axis line of any round columns that may be involved. Concerning cylinders with sweepback angles of 15° and 30°, this same sort of bow-shaped shock wave and the surfaces of the column make a small included angle. (When the angle of sweepback is 15°, the included angle is 1°. When the angle of sweepback is 30°, the included angle is 2°). Because of this fact, gas flow which follows the bow-shaped shock waves is inclined upward. The high pressure at the Y-point flows upward, and the downward influence on a flat plate is weakened. From the curves in Figure 8, it can be seen that, when the angle of sweepback is 15°, the curves defined by the heat transfer coefficients involved

still have troughs. Because of this, it is still possible to have a small, weak vortex.

The influence of inclined slopes on lateral lines are the same as those explained above. The only difference is that the influences are somewhat weaker (Figure 4).

5. Gas flows and the influence of Mach numbers. Mach numbers have an important influence on the peak values of heat flow. From formula (2) one can see that the influence of Mach numbers is in direct proportion with $M^{1.8}$. As far as lateral and lower flow heat transfer is concerned, the influence of Mach numbers have properties which are the same. Gas flow Mach numbers also influence the range of areas of interference. When Mach numbers are high, the range of interference areas is large (Figure 2). As far as long cylinders are concerned, $M = 6.6$, and the area of interference is smaller than 2.5D; moreover, when $M = 9$, interference areas are larger than 2.5D. In the case of short cylinders ($L/D = 0.25$), these areas increase from 1D to 1.2D.

When gas flow Mach numbers are high, the weakening and attenuation proceeding down the flow are relatively rapid, that is to say, the influences of these high Mach numbers on the lower parts of the flow are relatively strong. Concerning weakening and attenuation which is caused by sweepback when gas flow Mach numbers are high, the influence of such swept back configurations is strong. When $M = 9$, the peak value on the center line of the upper parts of the flow drops to one-sixth of the peak value for vertical cylinders when the sweepback angle is 30°. Moreover, when $M = 6.6$, it only drops to approximately one-fourth.

4. CONCLUSIONS

1. In the course of these experiments, we discovered that the highest rates of surface heat flow within the interference

areas of cylindrical protuberances are not located in the base section of the cylinders involved but in locations 0.1-0.15D from the base sections of these cylinders on the center line of the upper parts of the flow. Due to the fact that the density of the measurement points and the measurement process do not produce lateral heat conduction errors, the meausred peak values of heat transfer coefficient are much higher than the numerical values which have been determined outside of China from experiments and calculated from formulas. When $M = 9$, the peak values for heat transfer coefficients reach values as much as 46 times higher.

2. Swept back configurations are capable of making obvious reductions in the range of interference areas as well as of greatly lowering the maximum heat transfer coefficients. These effects are particularly obvious when Mach numbers are high. Moreover, forward inclined configurations are useless when it comes to heating environments.

3. Gas flow Mach numbers have important influences on the maximum heat transfer coefficient values. These maximum heat transfer coefficient values are directly proportional to M1.8. When Mach numbers are high, interference area ranges are expanded and there is a reduction and slowing down of the attenuation of the lower part of the flow.

4. When cylinder heights are larger than the corresponding cylinder diameters, the influence of height is extremely weak. When the height-to-diameter ratio is small than 1, the influence exerted by cylinder height is very large.

These experiments were completed in cooperation with the heat transfer team and the high pressure vacuum measurement team of the JF Laboratory. The Schlieren photography was taken by comrades Liu Fang and Hu Jin-ming.

REFERENCES

[1] Войженко Д. М., и другце, *Обтекание Цилиндрилеского препятетвия на пластина* сверхзвуковый потоком газа, и зв, *Акад. Наук, СССР Механика Жидкости и газа*, 1 (1966).

[2] Westkaemper, J. C., Turbulent boundary layer seperation ahead of cylinder, *AIAA J.* 6, 7(1968).

[3] Sedney, R. & Kitchens, C. W. Jr., Seperation ahead of protuberances in supersonic turbulent boundary layer, *AIAA. J.* 15, 4(1977).

[4] Price E. A., & R. L., Stallings Jr., Investigation of turbulent seperated flows in the vicinity of fin type protuberance at supersonic Mach numbers, NASA TN D-3804 (1967).

[5] Korkegi, R. H., Survey of viscous interactions associated with high Mach numbers flight, *AIAA J.*, 9, 5(1971).

[6] Burbank, P. B., Newlander, R. A. & Collins, I. R., Heat transfer and pressure measurements on a flate plate surface and heat transfer measurement on attached protuberance in a supersonic turbulent bounlary layer at Mach number of 2.65, 3.57 and 4.44, NASA TN D-1372 (1962).

[7] SAE Aerospace Applied Thermodynamics Manual, 2nd edition (1969).

[8] Truitt, R. W., Hypersonic turbulent boundary layer interference heat transfer in vicinity of protuberance, *AIAA J.*, 3, 9(1965).

[9] Yu Hong-rui and Li Zhong-fa "The uses of Thermoelectric Simulation in Surface Measurement of Heat Flow", Mechanics and Practical Applications, 2, 1 (1980)

[10] Nestler, D. E., et al., Heat transfer to step and cavities in hypersonic turbulent flow, *AIAA J.*, 7, 7(1969).

[11] George, A. R. & Roinecke, W. G., Conduction in thin-skinned heat transfer and recopery temperature models, *AIAA J.* 1, 8(1963).

Abstract

The results of heat tranfer rate measurements in the interaction region of a cylindrical protuberance is described. It is found that the maximum heat rate on the centerline does not occur at the foot of the cylinder but at a distance of 0.1 to 0.15 diameter of cylinder upstream from it. For a cylinder normal to the surface, the maximum heat transfer rate is 46 times that of flat plate value at Mach number 9, and 31 times at Mach number 6.6.

The effect of cylinder sweep on both the extent of interaction region and the maximum heat transfer rate is significant particularly at high Mach numbers. When backsweep angle varies from 0° to 30°, the maximum heat transfer rate decreases by a factor of about 6. For forward sweep, both the extent of the interaction region and the maximum heat transfer rate increase.

THE PROBLEM OF IGNITION IN A LAMINAR BOUNDARY LAYER OVER A HEATED PLATE*

Sun Bing-hua
(Qing Dao Gas Turbine Factory)

Figure 1 shows a high temperature inertia heated plate for a temperature T_o. The combustible mixture of gases which flows over this surface forms a laminar flow boundary layer. Where $x = x_1$, the combustible gases begin to ignite. This article is going to make use of differential equations in order to do research into this question.

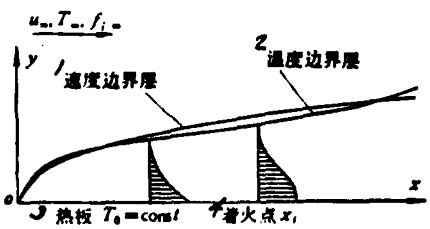

Figure 1. Ignition on a heated plate in a laminar flow boundary layer.

Key: 1--speed boundary layer; 2--temperature boundary layer; 3--heated plate; 4--ignition point

BASIC ASSUMPTIONS

1. The speed of the conflicting flows u_∞ is very small.
2. The direct proportion between the viscosity μ and the coefficient of thermal conductivity λ and the temperature T and the specific heat C_p is a constant.
3. The Prandtl number Pr and the Schmidt number Sc are equal and are constant.

*This article was received on April 8, 1978

4. The pressure gradient $\frac{dP}{dx} = 0$.

5. The temperature of the heated plate is T_o = cons t.

6. The speed of the second degree two molecular reaction can be represented as the reaction speed

$$W_i = K_{0i}\rho^2 f_i^2 \exp\left(-\frac{E}{RT}\right).$$

In this equation K_o is the speed constant for the reaction. f is the corresponding concentration. R is the normal gas constant. E is the reactivity. i represents the i-th type of component.

BASIC EQUATIONS

If we make use of the Howarth-Dorodnitzyn transformation, it is possible to take the basic equation for a compressible air flow and transform it into the basic equation for incompressible air flow, that is

$$\left.\begin{aligned}
&\frac{\partial u}{\partial x} + \frac{\partial v}{\partial y} = 0 \\
&u\frac{\partial u}{\partial x} + v\frac{\partial u}{\partial y} = \nu_\infty \frac{\partial^2 u}{\partial y^2} \\
&u\frac{\partial T}{\partial x} + v\frac{\partial T}{\partial y} = \frac{\nu_\infty}{\Pr}\frac{\partial^2 T}{\partial y^2} + \frac{Q_{xi}K_{0i}\rho f_i^2 \exp\left(-\frac{E}{RT}\right)}{C_p} \\
&u\frac{\partial f_i}{\partial x} + v\frac{\partial f_i}{\partial y} = \frac{\nu_\infty}{Sc}\frac{\partial^2 f_i}{\partial y^2} - K_{0i}\rho f_i^2 \exp\left(-\frac{E}{RT}\right)
\end{aligned}\right\} \quad (1)$$

In these quations, Q_x is the heat value. The corresponding boundary conditions are

$$\left.\begin{array}{l} y=0,\ u=v=0,\ T=T_0,\ \dfrac{\partial f_i}{\partial y}=0 \\ y\to\infty,\ u=u_\infty,\ T=T_\infty,\ f_i=f_{i\infty} \end{array}\right\} \quad (2)$$

From (1) and (2), if we carry out an integration, it is easy to obtain the differential for the energy equation and the diffusion equation involved. This takes the form given below, that is

$$\frac{d}{dx}\int_0^\infty u(T_\infty - T)dy = \frac{\nu_\infty}{\Pr}\left(\frac{\partial T}{\partial y}\right)_0 - \frac{Q_{si}K_{0i}}{C_p}\int_0^\infty \rho f_i^2 \exp\left(-\frac{E}{RT}\right)dy \quad (3)$$

$$\frac{d}{dx}\int_0^\infty u(f_{i\infty} - f_i)dy = \frac{\nu_\infty}{\mathrm{Sc}}\left(\frac{\partial f_i}{\partial y}\right)_0 + K_{0i}\int_0^\infty \rho f_i \exp\left(-\frac{E}{RT}\right)dy \quad (4)$$

In order to make the induction easy, take (3), (4) and convert them to a dimensionless form. In this way, make

$$U=\frac{u}{u_\infty},\ \eta=\frac{y}{\delta};\ \theta=\frac{T-T_\infty}{T_0-T_\infty},$$

$$\xi=\frac{y}{\beta};\quad F=\frac{f_i-f_{i\infty}}{f_{i0}-f_{i\infty}},\quad \zeta=\frac{y}{\gamma}.$$

In these equations, δ、β、γ respectively represent speed, temperature and the thickness of the concentration boundary layer. In this way, (3), (4) are transformed into the form

$$\frac{d}{dx}\left[\beta\int_0^1 \theta U d\xi\right] = -\frac{\nu_\infty}{\Pr u_\infty \beta}\left(\frac{\partial\theta}{\partial\xi}\right)_0 + \frac{\beta Q_{si}K_{0i}\rho_0 f_{i0}^2 \exp\left(-\dfrac{E}{RT_0}\right)}{C_p(T_0-T_\infty)u_\infty}\cdot I_n \quad (5)$$

$$\frac{d}{dx}\left[\gamma\int_0^1 FUd\zeta\right] = -\frac{\nu_\infty}{\mathrm{Sc}u_\infty\gamma}\left(\frac{\partial F}{\partial\zeta}\right)_0 + \frac{\beta K_{0i}\rho_0 f_{i0}^1 \exp\left(-\dfrac{E}{RT_0}\right)}{(f_{i\infty}-f_{i0})u_\infty}\cdot I_n \quad (6)$$

In these equations, I_n represents a differential, that is

$$I_n = \int_0^1 \frac{\rho}{\rho_0}\left(\frac{f_i}{f_{i0}}\right)^2 \exp\left[-\frac{E}{RT_0}\left(\frac{T_0}{T}-1\right)\right]d\xi \quad (7)$$

APPROXIMATION CROSS SECTIONS

On the basis of a Pohlhausen selection, as far as a flat plate defined by $\frac{dP}{dx} = 0$ is concerned, the speed cross section is

$$U = \frac{u}{u_\infty} = 2\eta - 2\eta^3 + \eta^4, \quad \eta = \frac{y}{\delta} \tag{8}$$

On the basis of the boundary conditions below, we select the temperature cross section, that is

$$\left.\begin{aligned} y = 0,\ T = T_0,\ \frac{\partial^2 T}{\partial y^2} &= -\frac{\Pr Q_{xi} K_{0i} \rho_0 f_{i0}^n \exp\left(-\frac{E}{RT_0}\right)}{\nu_\infty C_p} \\ y = \beta,\ T = T_\infty,\ \frac{\partial T}{\partial y} &= \frac{\partial^2 T}{\partial y^2} = 0 \end{aligned}\right\}$$

We can introduce a non-dimensional temperature deformation parameter, that is

$$H(x) = \frac{\Pr Q_{xi} K_{0i} \rho f_{i0}^n \exp\left(-\frac{E}{RT_0}\right)}{C_p (T_0 - T_\infty) \nu_\infty} \cdot \beta^2 \tag{9}$$

If we make use of a cross section determining precise values for tempeature and consisting of more than four quantities, the result is

$$\theta = \frac{T - T_\infty}{T_0 - T_\infty} = 1 - \frac{1}{6}(12 - H)\xi - \frac{H}{2}\xi^2 + \frac{1}{2}(4 + H)\xi^3 - \frac{1}{6}(6 + H)\xi^4, \quad \xi = \frac{y}{\beta} \tag{10}$$

The ignition condition is x = x_i and $\left(\frac{\partial T}{\partial y}\right)_0 = 0$
From (10) it is possible to obtain the temperature deformation parameter for the moment of ignition which is

$$H(x_i) = 12. \tag{11}$$

"The significance of the temperature deformation parameters is that, when H increases with x, the temperature fields involved give rise to violent deformations. Obviously, this is a result due to the liberation of heat in chemical reactions. The temperature fields involved are drawn out in Fig. 2.

The selection of concentration profiles by the use of similar methods is as presented below:

$$F = \frac{f_{i\infty} - f_i}{f_{i\infty} - f_{i0}} = 1 - \frac{1}{6}(12 - c)\zeta - \frac{c}{2}\zeta^2 + \frac{1}{2}(4 + c)\zeta^3 - \frac{1}{6}(6 + c)\zeta^4, \quad \zeta = \frac{y}{\gamma}. \tag{12}$$

In this equation, c is the concentration deformation parameter, that is

$$C(x) = \frac{\mathrm{Sc}\, K_{0i}\rho_0 f_{i0}^2 \exp\left(-\frac{E}{RT_0}\right)}{(f_{i\infty} - f_{i0})\nu_\infty} \cdot \gamma^2 \tag{13}$$

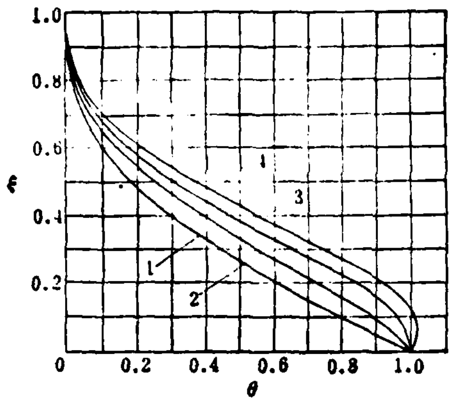

Figure 2. Temperature cross section

$1-H=0,\ 2-H=6,\ 3-H=12\ \ 4-H=18.$

If one is speaking from the point of view of an inertia heated plate, the boundary condition for concentration is $\left(\frac{\partial f_i}{\partial y}\right)_0=0$ At this time, on the basis of the concentration cross seciton, there must be

$$C(x)=12. \tag{14}$$

In this type of situation, f_{io} is a function of x, or it is a function of H. On the basis of the definition for H, Equation (9) as well as (14) show the relationship

$$\left.\begin{aligned} N &= \frac{f_{i0}}{f_{i\infty}} = 1 - HM(\Lambda - 1), \\ \Lambda &= \frac{T_0}{T_\infty},\ M = \frac{C_p T_\infty}{12 Q_{xi} f_{i\infty}}. \end{aligned}\right\} \tag{15}$$

In this case, it is necessary to point out that the concentration boundary which is used by Dooley is f_{io} = const. Morever, that used by Toong is $\left(\frac{\partial f_i}{\partial y}\right)_0=0$. The solutions for these are both numerical solutions. Obviously, as far as inertia heated plates are concerned, the second type of boundary condition is relatively reasonable.

APPROXIMATE SOLUTION EQUATIONS

As far as the boundary condition $\left(\frac{\partial f_i}{\partial y}\right)_0 = 0$ is concerned, f_{io} is a function of x. One can take the temperature deformation parameter and change it so that it is written in the form

$$H = nN^4\beta^4, \quad n = \frac{\Pr Q_{xi} K_{0i} \rho_0 f_{i\infty} \exp\left(-\frac{E}{RT_0}\right)}{C_p(T_0 - T_\infty)\nu_\infty} \tag{16}$$

If one takes the corresponding cross section and substitutes it into Equation (5), then one can obtain

$$\frac{d}{dx}[\beta(h_1 + h_2 H)] = \frac{1}{r}\frac{\nu_\infty}{\Pr u_\infty \beta}(12 - H) + \frac{\nu_\infty}{\Pr u_\infty} nN^4\beta \cdot I_n \tag{17}$$

In this equation h_1 and h_2 are both functions of $r = \frac{\beta}{\delta}$, and when they are differentiated, one gets the following

when $r \leqslant 1$

$$\left.\begin{aligned} h_1 &= \frac{2}{15}r - \frac{3}{140}r^3 + \frac{1}{180}r^4 \\ h_2 &= \frac{1}{180}r - \frac{1}{840}r^3 + \frac{1}{3024}r^4 \end{aligned}\right\} \tag{18}$$

when $r \geqslant 1$

$$\left.\begin{aligned} h_1 &= \frac{3}{10} - \frac{3}{10r} + \frac{2}{15r^2} - \frac{3}{140r^4} + \frac{1}{180r^5} \\ h_2 &= \frac{1}{120} - \frac{1}{90r^2} + \frac{1}{84r^3} - \frac{3}{560r^4} + \frac{1}{1080r^5} \end{aligned}\right\} \tag{18a}$$

These calculations demonstrate that, within the range r = 0.7 - 1.8 the difference between the two equations can be completely ignored and not taken into consideration for purposes of these calculations. In this way, one can make use of (18) later because of the fact that it is relatively easy to use.

The differential I_n becomes

$$\begin{aligned} I_n = \int_0^1 &\left[\frac{1}{1 + (\Lambda - 1)\theta}\right]\left[\frac{1}{N} - \left(\frac{1}{N} - 1\right)F\right]^2 \\ &\times \exp\left[-\frac{E}{RT_0}\frac{(\Lambda - 1)(1 - \theta)}{1 + (\Lambda - 1)\theta}\right] d\xi \end{aligned} \tag{19}$$

If one takes (17) and carries its simplification a step further, one obtains

$$\frac{dH}{d\bar{x}} + l\frac{dr}{d\bar{x}} = g\left[4 + 2H\left(I_n - \frac{1}{6}\right)\right]. \tag{20}$$

$$
\left.\begin{aligned}
l &= \frac{2H(h_3 + h_4H)[1 + HM(\Lambda - 1)]}{h_1 + [h_1M(\Lambda - 1) + 3h_2]H - h_2M(\Lambda - 1)H^2}, \\
g &= \frac{[1 - HM(\Lambda - 1)]^3}{h_1 + [h_1M(\Lambda - 1) + 3h_2]H - h_2M(\Lambda - 1)H^2},
\end{aligned}\right\} \tag{20a}
$$

$$
h_3 = \frac{dh_1}{dr}, \quad h_4 = \frac{dh_2}{dr}. \tag{20b}
$$

The non-dimensional coordinates in these equations are

$$
\tilde{x} = \frac{x}{\left(\frac{\Pr u_\infty}{n\nu_\infty}\right)}. \tag{20c}
$$

Equation (20) is nothing else than an approximate solution equation for H and r. It is still necessary to supplement the situation with one more equation. From the definition of H, one can get the equation (16), that is

$$
H = nN^2\beta^2 = nN^2r^2\delta^2
$$

On the basis of the Karman-Pohlhausen approximate solution, the thickness of the speed boundary layer is

$$
\delta = 5.83 \frac{x}{\sqrt{\frac{u_\infty x}{\nu_\infty}}},
$$

If one substitutes the equation above, then he gets

$$
H = 34 \Pr \tilde{x}[1 - HM(\Lambda - 1)]^2 r^2. \tag{21}
$$

This is nothing else than the supplementary equation which we required. The initial conditions for this are as follows:

when $$\tilde{x} = 0, \; H = 0, \; r = r_0 = \frac{1}{\sqrt[3]{\Pr}}. \tag{22}$$

The condition which we are considering, that is, $r_0 = \frac{1}{\sqrt[3]{\Pr}}$ is obtained in the following way. We took Equation (21) and substituted into Equation (20), that is

$$
\frac{dr}{d\tilde{x}} = \left\{ g\left[4 + 2H\left(l_* - \frac{1}{6}\right)\right] - 34 \Pr [1 - HM(\Lambda - 1)]^2 r^2 - 34 \Pr \tilde{x} \frac{d}{d\tilde{x}}\{[1 - HM(\Lambda - 1)]^2 r^2\} \right\} \Big/ l
$$

In the equation above, when $\tilde{x} \to 0$, $H \to 0$, and the denominator $l \to 0$ the numerator must $\longrightarrow 0$, and in such a case, one gets

$$\frac{4}{h_1} - 34\,\mathrm{Pr}\, r_0^3 = 0$$

This equation is an equation which solves for the ratio r of the speed boundary layer thickness and the temperature boundary layer thickness when no combustion reactions are taking place. The value of this is $r_0 = \frac{1}{\sqrt[3]{\mathrm{Pr}}}$.

It should be explained that it is only when one selects $\frac{\beta}{\gamma} = 1$ that it is possible to make calculations of (19) with relative ease. The analysis involved is the same type as that used in the cases of (18) and (18a). The error which is given rise to by the use of this method is very small. In this way, we can then forget about Equation (6). Otherwise, it would be necessary to take Equation (6) into consideration, and this would make the problems involved much more complicated.

REFERENCES

[1] Toong, T. Y., Lgnition and Combustion in a Laminar Boundary Layer Over a Hot Surface, Sixth Symposium (International) on Combustion, New Haven, Conn., Aug. (1956), 19—24.

[2] Toong. T. Y., Flame Stabilization in Boundary Layers, 12th Meeting AGARD Combustion and *Propulsion Panel*, Washington, D. C., Nov. (1957), 18—26.

[3] Donald A. Dooley, Ignition in the Laminar Boundary Layer of a Heated plate, Heat Transfor and Fluid Mechanics Institute (1957).

[4] Ziemer and Cambel, Flame Stabilization in the Boundary Layer of Heated Plates Jet Propulsion, 28(1958).

[5] Dorodnitsyn, A., Laminar Boundary Layers in Compressible Fluids, Dokl. Akad, Nauk S.S.S.R. 34, 8(1952), 218—219.

[6] Schlichting, H., Boundary-Layer Theory. Sixth Edition, London (1968).

Abstract

The problems of ignition and combustion in laminar boundary layer over a heated plate are studied by means of an approximate method analogous to that developed by Kármán and Pohlhausen in their investigation of the separation of laminar boundary layer over a plate.

The basic partial differential equations are transformed into an ordinary differential equation of the first order for the temperature deformation factor *H*, and the calculation of integral in is a prerequisite to resolving the equation. The introduction of factor *H* is covenient in determining the ignition distance since *H* equals 12 at the ignition point on the plate

DATE
LMED
8